

# Absence of Ferromagnetism in VSe<sub>2</sub> Caused by Its Charge Density Wave Phase

Adolfo O. Fumega,<sup>\*,†,‡</sup> M. Gobbi,<sup>§</sup> P. Dreher,<sup>§</sup> W. Wan,<sup>§</sup> C. González-Orellana,<sup>§</sup> M. Peña-Díaz,<sup>§</sup> C. Rogero,<sup>§,¶</sup> J. Herrero-Martín,<sup>||</sup> P. Gargiani,<sup>||,¶</sup> M. Illyn,<sup>§</sup> M. M. Ugeda,<sup>§</sup> Victor Pardo,<sup>\*,†,‡,¶</sup> and S. Blanco-Canosa<sup>\*,⊥,#</sup>

<sup>†</sup>Departamento de Física Aplicada, Universidade de Santiago de Compostela, Campus Sur s/n, E-15782 Santiago de Compostela, Spain

<sup>‡</sup>Instituto de Investigaciónes Tecnológicas, Universidade de Santiago de Compostela, Campus Sur s/n, E-15782 Santiago de Compostela, Spain

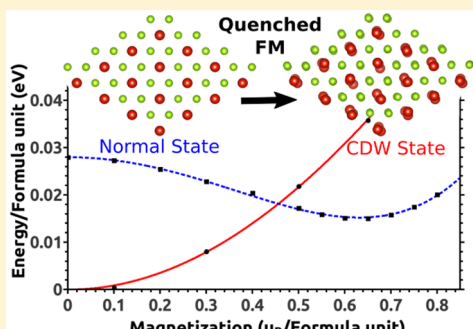
<sup>§</sup>Centro de Física de Materiales (CSIC UPV/EHU), Paseo Manuel de Lardizábal, 5, E-20018 Donostia San Sebastián, Gipuzkoa, Spain

<sup>||</sup>ALBA Synchrotron Light Source, Cerdanyola del Vallès, 08290 Barcelona, Catalonia, Spain

<sup>⊥</sup>Donostia International Physics Center, DIPC, 20018 Donostia-San Sebastian, Basque Country, Spain

<sup>#</sup>IKERBASQUE, Basque Foundation for Science, 48013 Bilbao, Basque Country, Spain

**ABSTRACT:** How magnetism emerges in low-dimensional materials such as transition metal dichalcogenides at the monolayer limit is still an open question. Herein, we present a comprehensive study of the magnetic properties of single-crystal and monolayer VSe<sub>2</sub>, both experimentally and *ab initio*. Magnetometry, X-ray magnetic circular dichroism (XMCD), and *ab initio* calculations demonstrate that the charge density wave in bulk stoichiometric VSe<sub>2,0</sub> causes a structural distortion with a strong reduction in the density of states at the Fermi level, prompting the system toward a nonmagnetic state but on the verge of a ferromagnetic instability. In the monolayer limit, the structural rearrangement induces a Peierls distortion with the opening of an energy gap at the Fermi level and the absence of magnetic order. Control experiments on defect-induced VSe<sub>2-δ</sub> single crystals show a breakdown of magnetism, discarding vacancies as a possible origin of magnetic order in VSe<sub>2</sub>.



## INTRODUCTION

Since the discovery of graphene,<sup>1</sup> much scientific effort is concentrated on the characterization of purely two-dimensional (2D) materials. In particular, the family of layered transition metal dichalcogenides (TMDs, MX<sub>2</sub>; M = Nb, Ti, V,··· X = S, Se, Te) is attracting great attention<sup>2–5</sup> since emergent phenomena driven by novel electronic, optical, and quantum many-body properties at the 2D limit could lead to new applications.<sup>6</sup> Control over the material thickness down to the monolayer limit has been accurately achieved by mechanical exfoliation,<sup>7</sup> chemical vapor deposition, and layer-by-layer molecular beam epitaxy (MBE),<sup>8,9</sup> revealing that collective quantum ground states, coherent modulation of electronic periodicities,<sup>10</sup> superconductivity,<sup>11</sup> and optoelectronic and valley excitonic physics<sup>12–15</sup> survive down to the atomic scale.

Nevertheless, long-range magnetic ordering in low dimensions has been elusive for decades. Theoretically, the Mermin–Wagner theorem<sup>16</sup> prohibits long-range magnetic order in the 2D isotropic Heisenberg model at finite temperatures if the system is spin-rotational invariant. Nevertheless, Ising-type ferromagnetism has been observed in a purely 2D material,<sup>17–19</sup> paving the path for future spintronic applications. Moreover,

simple defects in a host lattice strongly alter both macroscopic and local properties of the system. Magnetic order from disorder has been observed to emerge in superconducting cuprates upon substitution of nonmagnetic ions by spinless impurities,<sup>20</sup> by Kondo systems,<sup>21</sup> and in highly oriented pyrolytic graphite (HOPG),<sup>22</sup> demonstrating that grain boundaries, vacancies, and point defects can act as magnetic nuclei in a nonmagnetic matrix.<sup>23</sup>

Recently, a strong ferromagnetic (FM) signal at room temperature has been reported at the monolayer limit of the 2D van der Waals system VSe<sub>2</sub>,<sup>24</sup> broadening the spectrum of 2D materials hosting magnetism in the ultrathin limit.<sup>25,26</sup> Van der Waals stacked layers of VSe<sub>2</sub> consist of 6-fold-coordinated V atoms crystallizing in a trigonal (1T) structure (space group *P3m1* in the normal state, NS, see Figure 1(a)). For many TMDs,<sup>27,28</sup> both transport<sup>29,30</sup> and diffraction data<sup>31</sup> show that bulk VSe<sub>2</sub> develops a 3D charge density wave (CDW) below  $T_{CDW} \sim 110$  K<sup>32</sup> with a new commensurate  $4a \times 4a \times 3c$  lattice

Received: September 18, 2019

Revised: October 22, 2019

Published: October 22, 2019

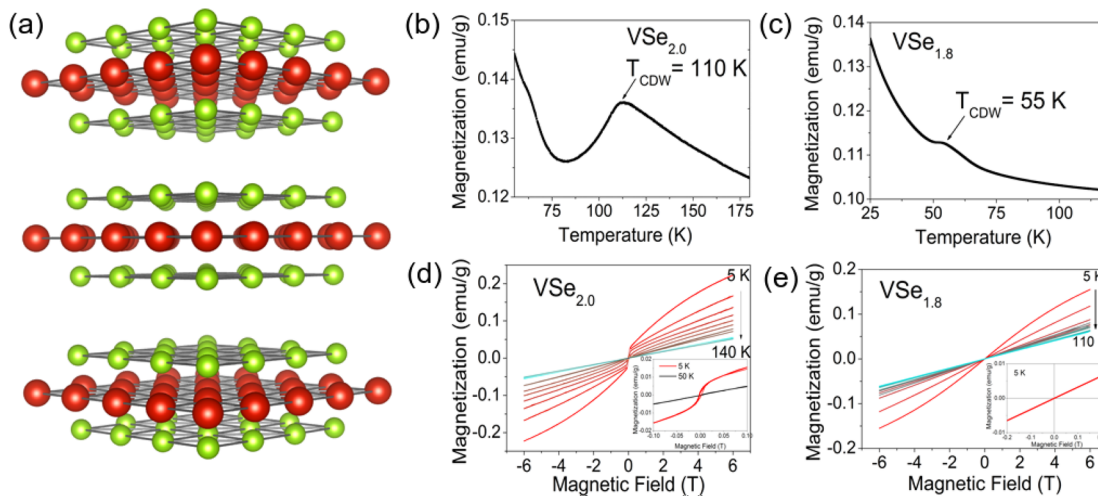


**Figure 1.** (a) Layered structure of  $\text{VSe}_2$  in the  $P\bar{3}m1$  space group. V atoms are represented as red spheres, and Se atoms are shown in green. (b,c) Temperature dependence of the magnetization for stoichiometric  $\text{VSe}_{2.0}$  and Se-deficient  $\text{VSe}_{1.8}$  single crystals. The charge density wave transition temperature ( $T_{\text{CDW}}$ ) is signaled by a kink in the magnetization curve. (d,e) Magnetization vs field for  $\text{VSe}_{2.0}$  and  $\text{VSe}_{1.8}$  single crystals. Inset: zoom-in of the low-field magnetization highlighting the small magnetic signal for  $\text{VSe}_{2.0}$ , not observed in  $\text{VSe}_{1.8}$ .

periodicity.<sup>29,33,34</sup> A pseudogap appears at the Fermi surface,<sup>35</sup> and the system remains paramagnetic.<sup>29,35–37</sup> Remarkably,  $T_{\text{CDW}}$  increases at the monolayer limit,<sup>7</sup> and a gap opens at the Fermi level<sup>9</sup> with a controversial magnetic behavior for exfoliated<sup>7</sup> and MBE-grown monolayers.<sup>24</sup> However, a consistent picture about the microscopic origin of magnetism in  $\text{VSe}_2$  and the development of FM order in this nonmagnetic material in 2D is still lacking. In part, this is a consequence of the proximity to electronic and magnetic instabilities which can balance the competition between ground states in the 2D limit. Angle-resolved photoemission (ARPES)<sup>10</sup> and scanning tunneling microscopy (STM)<sup>8</sup> have revealed an electronic reconstruction of single-layer  $\text{VSe}_2$  compared with the bulk counterpart, without a detectable FM exchange splitting, casting doubts on whether magnetism originates from an induced band structure spin splitting caused by dimensionality reduction or extrinsic defects come into play. Indeed, previous density functional theory (DFT) calculations<sup>38–41</sup> found a FM ground state for both bulk and single-layer  $\text{VSe}_2$ . However, these DFT calculations do not take into account the effect of the CDW structure, and hence, the electronic reconstruction and the effect of impurities are largely overlooked.

In order to shed light on the nature of the magnetic ground state in  $\text{VSe}_2$ , we have carried out a comprehensive theoretical and experimental study of bulk single-crystal and monolayer  $\text{VSe}_2$ . We report that, due to the reduction of the density of states (DOS) at the Fermi level caused by the opening of the CDW pseudogap, bulk  $\text{VSe}_2$  is close to a ferromagnetic instability, which cannot be induced by defects or vacancies. Besides, monolayer  $\text{VSe}_2$  shows a Peierls-like distortion that opens a gap at the ultrathin limit, preventing the system from developing a long-range FM order, in agreement with recent reports.<sup>10</sup>

## EXPERIMENTAL AND COMPUTATIONAL METHODS

Single crystals of  $\text{VSe}_{2.0}$  and  $\text{VSe}_{1.8}$  were grown by chemical vapor deposition following previous reports.<sup>30</sup> A 5% excess of Se for  $\text{VSe}_{2.0}$  and stoichiometric V:Se (1:2) for  $\text{VSe}_{1.8}$  was used during the synthesis. The V:Se ratio was measured by energy-dispersive X-ray spectroscopy (EDX). Single-layer  $\text{VSe}_{2.0}$  was

grown by MBE on an epitaxial bilayer graphene on silicon carbide (Si-C) and highly oriented pyrolytic graphite (HOPG) substrates in an ultrahigh vacuum chamber with a base pressure of  $\sim 1 \times 10^{-9}$  and 250 °C. After the growth, 3 min postannealing in a Se-rich atmosphere was carried out to fill in the Se vacancies. A Se capping layer was deposited after cooling to prevent oxidation and was *in situ* evaporated for XMCD experiments. Magnetic measurements on Se-capped  $\text{VSe}_2$  monolayers grown on diamagnetic bilayer graphene/SiC were carried out in a SQUID magnetometer up to 7 T. X-ray magnetic circular dichroism (XMCD) at the  $\text{V } L_{2,3}$ -edge up to 6 T was performed at the BOREAS beamline at the ALBA synchrotron.<sup>42</sup> Normal and grazing incidence geometries are referred to the 90° and 20° angle between the beam and sample surface, the latter being more sensitive to in-plane magnetization, and the magnetic field is always parallel to the beam direction. Cluster calculations were carried out using crystal field theory implemented in the QUANTY code<sup>43,44</sup> for the atomic-like  $2p^6-3d^5 \rightarrow 2p^5-3d^{5+1}$  transitions. First-principles DFT *ab initio* electronic structure calculations<sup>45,46</sup> were performed using an all-electron full potential code (WIEN2K<sup>47</sup>). The exchange-correlation term for the bulk structure was the generalized gradient approximation (GGA) in the Perdew–Burke–Ernzerhof<sup>48</sup> scheme. The LDA +U method was used for the 2D case.<sup>49</sup> The calculations were carried out with a converged  $k$ -mesh and a value of  $R_{\text{mt}}K_{\text{max}} = 7.0$  and an  $R_{\text{mt}}$  value of 2.12 au for both V and Se. Transport properties were obtained with the BoltzTrap2 code<sup>50</sup> using a denser  $k$ -mesh, solving the Boltzmann transport equation within the constant scattering time approximation.

## RESULTS

The paper is organized as follows: first, we present the experimental and theoretical results obtained for bulk  $\text{VSe}_2$ , followed by showing the results for the system at the monolayer limit.

**Bulk  $\text{VSe}_2$ .** Plotted in Figure 1(b,c) are the temperature dependencies of the magnetization for  $\text{VSe}_{2.0}$  and  $\text{VSe}_{1.8}$  single crystals. Following previous reports,<sup>29,30</sup> the CDW transition is identified as a kink in the magnetic susceptibility, at 110 K for  $\text{VSe}_{2.0}$  and 55 K for  $\text{VSe}_{1.8}$ , evidencing the drop in transition

temperature upon introducing Se defects. Interestingly, the field dependence of the magnetization shows s-shape magnetic behavior for  $\text{VSe}_{2.0}$  (Figure 1d, inset) but is absent in single crystals of  $\text{VSe}_{1.8}$  (Figure 1e). Nevertheless, neither the magnetization of  $\text{VSe}_{2.0}$  nor  $\text{VSe}_{1.8}$  saturates at 6 T. The small magnetic behavior observed in  $\text{VSe}_{2.0}$  could arise from Kondo impurities<sup>51</sup> or phase slippage of the CDW.<sup>52</sup>

To identify the source of magnetism in  $\text{VSe}_{2.0}$  single crystals, we have carried out X-ray magnetic circular dichroism (XMCD) at the  $\text{V } L_{2,3}$  edge at 6 T (Figure 2). As shown in Figure 2(b), a

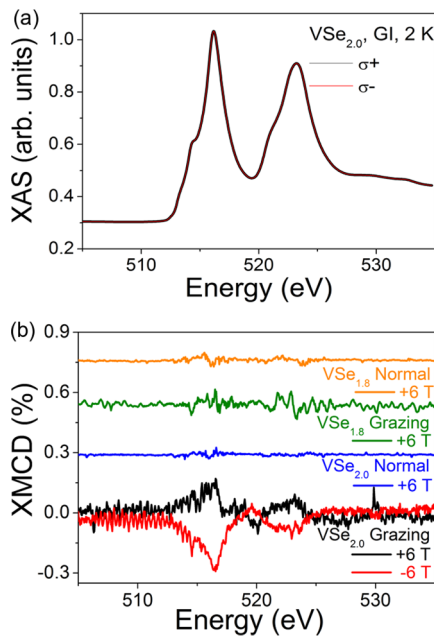


**Figure 2.** (a) XAS spectra for single-crystal  $\text{VSe}_{2.0}$  with circular positive ( $\sigma^+$ ) and negative ( $\sigma^-$ ) polarized light at 2 K, 6 T, and grazing incidence geometry (70° off with respect to the  $c$ -axis). (b) XMCD spectra for  $\text{VSe}_{2.0}$  and  $\text{VSe}_{1.8}$  single crystals at 2 K, 6 T, and normal (NI) and grazing (GI) incidence geometries. Only a small dichroic signal is discernible at GI.

small XMCD signal, defined as  $(\sigma^+ - \sigma^-)$ , can only be detected in  $\text{VSe}_{2.0}$  at the  $L_{2,3}$  in grazing incidence geometry (GI) at 6 T, suggesting that small moments are in-plane aligned. On the other hand, no significant dichroic signal is detected in  $\text{VSe}_{1.8}$  for normal and grazing incidence geometries. Comprehensive transport data highlighted the Kondo effect in  $\text{VSe}_{2.0}$  single crystals below 40 K;<sup>51</sup> thus, the small magnetic dichroism at the  $\text{V } L_{2,3}$  edge can be assigned to Kondo impurities. Nevertheless, the small XMCD signal precludes us to retrieve a hysteresis loop from the magnetic dichroism experiments. Further, the introduction of Se vacancies seems to be detrimental to magnetism.

In order to obtain a deep understanding of the electronic and magnetic ordering in single crystals of  $\text{VSe}_{2.0}$ , we have carried out *ab initio* calculations, both in the normal (NS) and CDW state. ARPES and X-ray diffraction<sup>29</sup> have found a 3-dimensional CDW below 110 K, leading to the opening of a pseudogap at the Fermi level at  $(\frac{1}{4}, \frac{1}{4}, \frac{1}{3})$  reciprocal lattice units.<sup>53</sup> To take this into account in our calculations, we have computed a  $4a \times 4a \times 3c$  supercell. Therefore, the introduction of a periodic lattice distortion may affect the calculated DOS at the Fermi level and hence the magnetic properties of this itinerant electron system.

Since  $\text{VSe}_2$  is an itinerant-electron system, one can make use of the phenomenological Stoner model<sup>54</sup> to analyze how close the system is to a magnetic instability. The Stoner theory compares the energy gained by the system via a spin splitting to the kinetic energy cost produced by displacing minority-spin electrons into a higher-energy majority-spin band. Only when the overall energy gets reduced, an itinerant electron system becomes spontaneously magnetic. The Stoner criterion states that

$$\text{Stoner criterion} \begin{cases} \text{FM, if } I \cdot \text{DOS}(E_F) > 1 \\ \text{Nonmagnetic, otherwise} \end{cases} \quad (1)$$

where  $I$  is the exchange energy between the Bloch d-band electrons, the so-called Stoner parameter.<sup>55</sup> Itinerant ferromagnets such as Fe, Ni, and Co present values of  $I \cdot \text{DOS}(E_F)$  ranging from 2.5 to 3.<sup>56</sup>

It follows from the energy ( $E$ ) vs magnetization ( $M$ ) curve that the bulk normal state yields a FM ground state with a broad minimum at around  $0.6 \mu_B$  per V atom (blue line in Figure 3c),

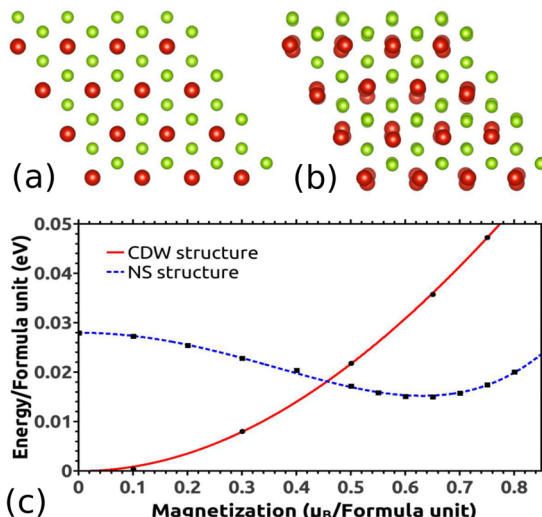


**Figure 3.** Top view of  $\text{VSe}_{2.0}$  bulk structures. V(Se) atoms are represented as big red (green) spheres. (a) NS structure in the  $P\bar{3}m1$  space group. (b) A modulated  $4a \times 4a \times 3c$  supercell of the CDW state. (c) Energy as a function of the magnetization for the bulk  $\text{VSe}_{2.0}$  for the NS structure (blue line) and CDW state (red line). The minimum at  $0.6 \mu_B$  per V atom indicates that the magnetic solution is the most stable in the NS. At low temperature, the minimum-energy configuration is a nonmagnetic CDW ground state.

with  $E = (1 - I \cdot \text{DOS}(E_F)) / \text{DOS}(E_F) M^2 + kM^4$ , and  $k$  is a fitting parameter independent of  $I$ .<sup>55</sup> The Fermi level is located at  $n = 0$ , where  $n$  is the number of electrons per formula unit and  $n > 0$  ( $n < 0$ ) implies hole (electron) doping, and the carrier concentration was calculated using a rigid-band approximation by integrating the total DOS of the nonmagnetic calculation. In Figure 4a, we show that the Stoner criterion for FM is satisfied for  $-0.5 < n < 0.5$ . However, any perturbation to this system leads to a small reduction in the DOS at the Fermi level and to a nonmagnetic state. Previous *ab initio* studies have shown that a reduction of the FM moment can be achieved by strain engineering.<sup>39</sup> Very recently, Zhang et al.<sup>57</sup> took advantage of the proximity of  $\text{VSe}_2$  to a magnetic ground state to engineer a FM heterostructure of  $\text{VSe}_2$  with a magnetic moment of about  $0.4 \mu_B$  per V atom, as we have predicted here. This finding

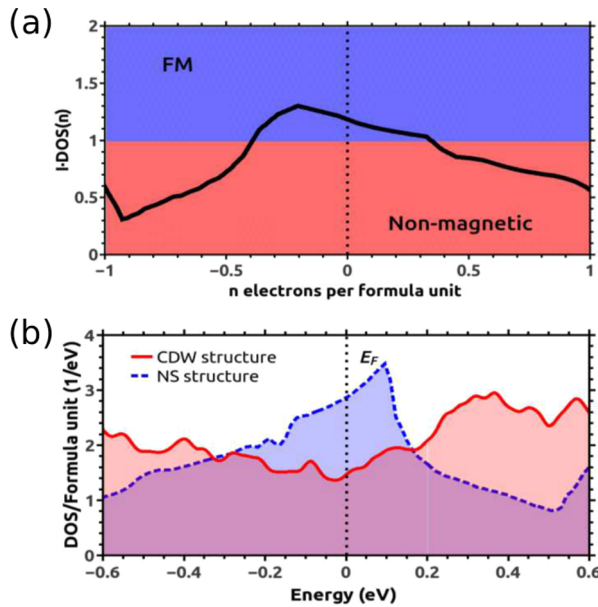


**Figure 4.** (a) Stoner criterion for the NS structure as a function of the number of electrons introduced per formula unit. In the NS, VSe<sub>2</sub> is FM but close to a nonmagnetic state. (b) DOS around the Fermi level for the bulk structures. Red (blue): DOS of the CDW (NS) state, showing a reduction of the DOS in the CDW state and the breakdown of the magnetism in the charge-ordered state.

highlights that monolayers of VSe<sub>2</sub> can be manipulated to tailor new magnetic ground states.

The optimized atomic positions at low temperature (CDW state), taking into account the new lattice periodicity,<sup>29</sup> are plotted in Figure 3b, showing that the short-range hexagonal symmetry is lost. The CDW structure calculated *ab initio* is 28 meV per formula unit more stable than the NS structure resulting in a strong reduction of the DOS at the Fermi level (Figure 4b) and a quenching of the FM moment as compared with the NS (Figure 3c).

Experimentally, a significant enhancement in the Seebeck effect is observed at the transition from the NS at high temperatures to the CDW state below 110 K, due to the opening of a pseudogap at the Fermi level. In Figure 5 the computed thermopower of both the NS (blue dashed line) and the CDW (red line) structures is compared to the ones in the literature<sup>30</sup>

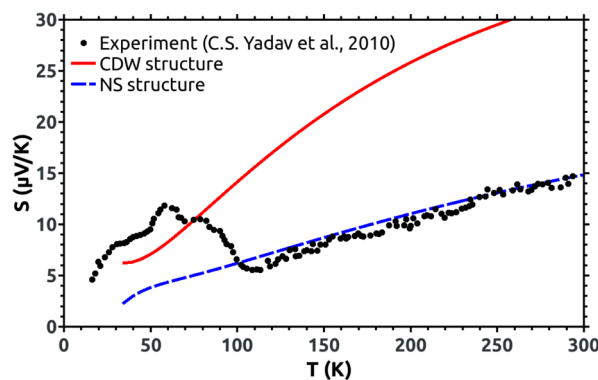


**Figure 5.** Thermopower as a function of temperature for bulk VSe<sub>2</sub>. The black points show the experimental measurements from ref 30. The red and blue lines show the calculated thermopower for the  $4a \times 4a \times 3c$  supercell (CDW state) and for the  $P\bar{3}m1$  cell (normal state).

(black points), evidencing that the relaxed structure can be modeled reasonably well with the CDW state found experimentally. Despite the coarse fitting at low temperature, an enhancement of the thermopower with respect to the NS is also obtained in the theoretical simulations within the constant scattering time approximation. This is further evidence for the reliability of modeling bulk VSe<sub>2</sub> in its CDW phase using a  $4a \times 4a \times 3c$  supercell.

**Monolayer VSe<sub>2</sub>.** Figure 6(a,b) shows the atomic force microscopy (AFM) image of high-quality monolayer VSe<sub>2,0</sub> grown on HOPG and Si-C, respectively, with typical heights of 6 Å. The field dependence of the magnetization ( $M[H]$ ) at 300 and 5 K for VSe<sub>2,0</sub> grown on the Si-C substrate is presented in Figure 6(c). The magnetic curves show a negative slope characteristic of the diamagnetic signal from the Si-C substrate, without indications of saturation or hysteresis, ruling out any magnetism coming from the VSe<sub>2,0</sub> monolayers, at least within the limit of detection of our setup. This is confirmed in Figure 6(d) after the subtraction of the magnetic signal of the Si-C substrate. Besides, XMCD at 6 T shows a featureless magnetic dichroism in normal or grazing incidence, as shown in Figure 6(f). Here, we point out that similar magnetic dichroism has been recently reported for spin-frustrated monolayers of VSe<sub>2</sub>.<sup>58</sup> In addition, a careful comparison between the XAS spectra of the single crystals and the monolayer also reveals a broadening of the  $L_3$  edge in the ultrathin limit, presumably as a consequence of the electronic reconstruction in the 2D limit.

To estimate the theoretical dichroism expected for a  $d^1$  system, we have carried out cluster calculations in the octahedral and trigonal crystal field for the atomic-like 3d transitions using QUANTY. The code incorporates the intra-atomic 3d–3d and 2p–3d magnetic exchange interactions, the atomic 2p and 3d spin-orbit couplings, and local crystal field parameter and Coulomb energies (Slater integrals) obtained within the Hartree–Fock approximation.<sup>59</sup>

Figure 6f and 6(g,h) show the experimental and the simulated isotropic spectrum, defined as  $\sigma^+ + \sigma^-$  as a function of the crystal field  $10D_q$  expected for spin- $\frac{1}{2}$  in trigonal and octahedral symmetries. To simulate the monolayer VSe<sub>2</sub> spectra, we used 40% of the atomic values of the Slater integrals in the  $O_h$  and  $C_{3v}$  symmetries of the V sites. As shown in Figure 6(g,h), the crystal field calculations for spin- $\frac{1}{2}$  V<sup>4+</sup> reveal a finite, but crystal-field dependent,  $10D_q$  magnetic dichroism. Strain effects induced by the HOPG and SiC graphene, which might alter the crystal field parameter, are found to be negligible in 2D monolayer TMDs. Therefore, the absence of magnetic dichroism in single-layer VSe<sub>2,0</sub> points to a strong electronic renormalization at the ultrathin limit. In fact, screening effects are enhanced with respect to the bulk VSe<sub>2,0</sub>, thus leading to an additional renormalization of the DOS. Indeed, the CDW phase is observed at  $T_{\text{CDW}}^{2D} > T_{\text{CDW}}^{3D}$ ,<sup>7</sup> revealing an enhancement of the electron–electron and electron–phonon interactions in 2D. Furthermore, the hopping parameter,  $t$ , between layers vanishes, and hence, the ratio between the on-site Coulomb repulsion and hopping,  $U/t$ , increases.

Following ARPES experiments,<sup>8,10,60</sup> the ground state of monolayer VSe<sub>2</sub> is characterized by an energy gap. However, the electronic modulation of the CDW remains under discussion.<sup>8–10</sup> Therefore, our aim within the following DFT calculations will be to explain the physical mechanism that undergoes the monolayer rather than looking for perfect agreement with controversial experimental data. We present

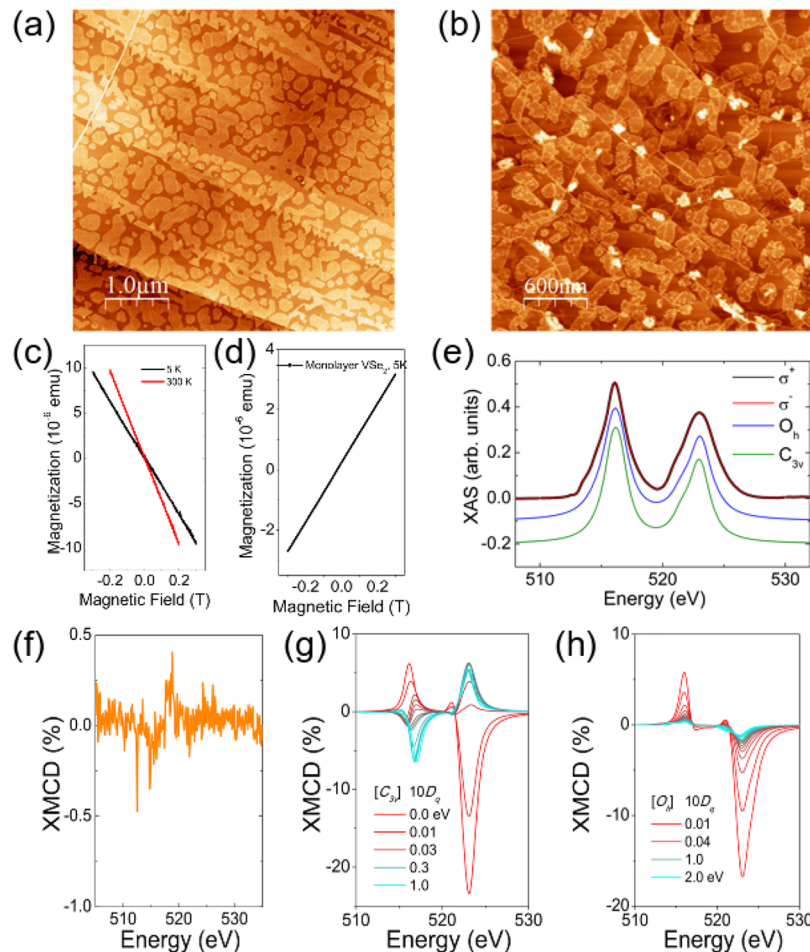


**Figure 6.** (a,b) AFM images of monolayer VSe<sub>2.0</sub> grown on HOPG and Si-C. (c) Magnetization vs field for VSe<sub>2.0</sub> on Si-C at 5 and 300 K. (d) Magnetization vs field for VSe<sub>2.0</sub> after the subtraction of the magnetic signal of the Si-C substrate. (e) Experimental XAS spectrum for ultrathin VSe<sub>2</sub> for  $\sigma^+$  (black) and  $\sigma^-$  (red) polarized light and the calculated isotropic XAS spectra for  $O_h$  and  $C_{3v}$  symmetries. (f) Experimental XMCD of VSe<sub>2.0</sub> on Si-C. (g,h) Calculated XMCD spectra for  $C_{3v}$  and  $O_h$  symmetries as a function of the crystal field splitting,  $10D_q$ .

calculations on a  $2a \times 2a$  supercell since it was computationally affordable. This will allow us to understand the possible electronic reconstructions that may occur in the 2D limit when a periodic lattice distortion takes place, shedding light on how both the FM quenching and the full-gap opening occur. In order to include the electron interactions that become stronger in the monolayer limit, we have performed LDA+U calculations. Figure 7(a) shows the evolution of the energy gap in the whole Brillouin zone as a function of  $U$  for a fully relaxed  $2a \times 2a$  supercell of the monolayer. At reduced values of  $U$ , a metallic FM structure is stable. However, for  $U$  greater than 2.7 eV a nonmagnetic CDW is formed, and consequently, an energy gap appears in the whole Brillouin zone, in agreement with experiments.<sup>10</sup> The calculated band structures for the non-magnetic monolayer NS and CDW states are shown in Figure 7(c). If no structural instability is present, the d-band crossing at the Fermi level and the high density of states (blue dashed line in Figure 7(d)) lead to a FM metallic state. Nevertheless, the structural transition associated with the CDW, depicted in Figure 7(b), drives the system toward a Peierls-like distortion with a tetramerization among 4 V atoms. A comparison between the DOS of the NS structures for both the bulk and the monolayer reveals that decreasing dimensionality increases the DOS at the Fermi level, and the bands become flatter due to the absence of the off-plane hopping. In general, for itinerant

systems, this would be a mechanism to enhance the stability of a FM phase. However, due to the CDW state, the four d-bands in the  $2a \times 2a$  supercell hybridize, forming two bonding and two antibonding bands (right side of Figure 7(b)), opening an energy gap (red line in Figure 7(d)) with a concomitant quenching of the FM moment.

Finally, in order to study *ab initio* the intrinsic effect of strain and Se vacancies in the monolayer limit, we have computed the DOS for different strain values and also carried out similar calculations including Se vacancies in a V:Se ratio similar to our single-crystal experiments (Figure 8). We have performed calculations in the NS and shown that the DOS is not substantially increased (mostly reduced) with respect to the unstrained stoichiometric NS monolayer VSe<sub>2.0</sub>. The effect of strain and Se vacancies can be seen in Figure 8(a,b), suggesting that neither strain nor Se vacancies will induce an intrinsic FM state in single-layer VSe<sub>2.0</sub>, as discussed above in our experiments for the bulk case.

## DISCUSSION AND CONCLUSIONS

Recently, transport and magnetometry experiments have reported a FM ground state for monolayers of VSe<sub>2</sub> grown on different substrates.<sup>24</sup> This is in agreement with previous DFT calculations that have predicted the emergence of a FM ground state for monolayers of VX<sub>2</sub> (X = S, Se).<sup>38–41</sup> Our combination

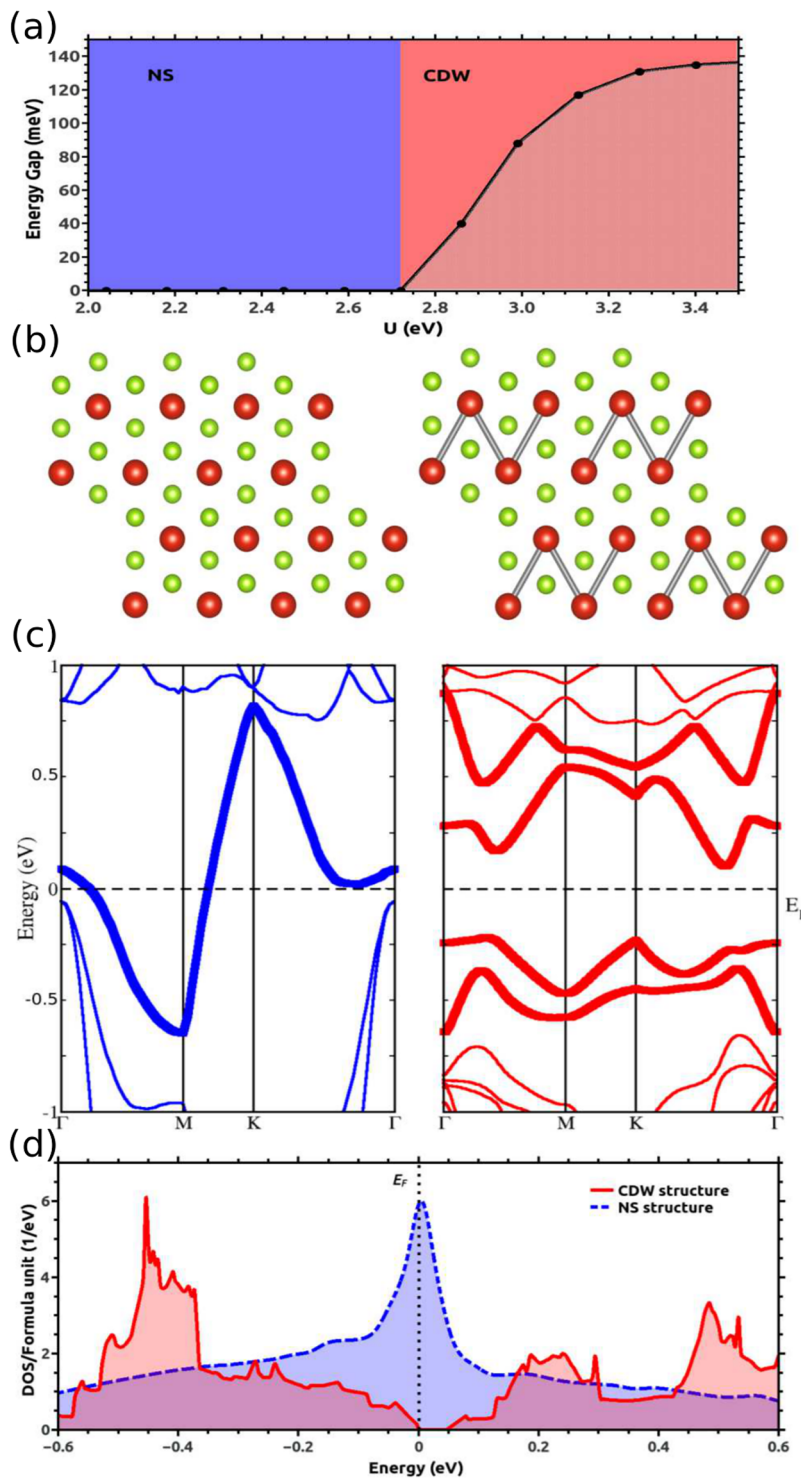


**Figure 7.** Results for the monolayer. (a) Mapping on  $U$ . The structure was fully optimized for each value of the Coulomb repulsion. At low values, the metallic FM NS structure is the most stable. For  $U > 2.7$  eV, a nonmagnetic gap opens, and the CDW stabilizes. (b) Structure schemes: NS on the left: each V atom has 6 neighbors at the same distance. CDW on the right: a tetramer is formed in a  $2a \times 2a$  supercell. The tetramer bonds are depicted in gray. (c) Band structures: On the left the NS: a d-band crosses the Fermi level producing a FM metallic state. On the right the CDW: the tetramer forms two bonding and two antibonding bands, opening a gap and quenching the magnetic moment. (d) Comparison of the DOS of the NS monolayer VSe<sub>2</sub> (blue dashed line) with the CDW state (red line).

of experimental data, including magnetization and XMCD, find a small ferromagnetic signal for stoichiometric bulk VSe<sub>2,0</sub>, which may arise from V impurities intercalated in the van der Waals gap. Naively, one may think that this Kondo mechanism gets inoperative when reducing the dimensionality of VSe<sub>2,0</sub>

down to the ultrathin limit, since no van der Waals gap is present. Nonetheless, still impurities in the surface of the monolayer can produce a Kondo effect. In the bulk case, *ab initio* calculations show that a CDW phase of the periodicity found experimentally destroys magnetism and is the ground-state structure. Recently,

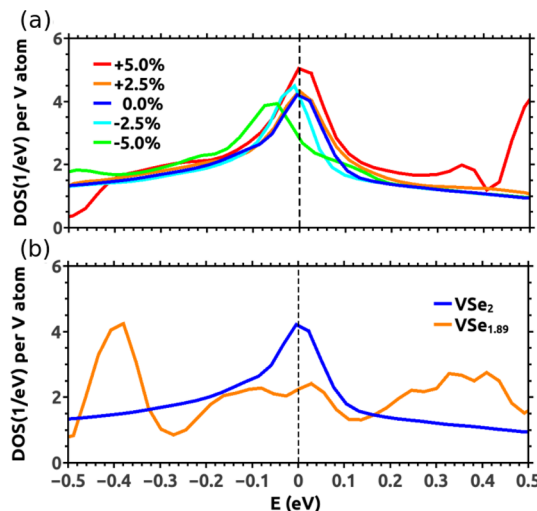


**Figure 8.** Calculated DOS for the monolayer. (a) DOS for different strain values of the lattice parameter for the monolayer single-unit cell. A substantial change in the DOS at the Fermi level is not observed. (b) Effect of Se vacancies on VSe<sub>2</sub> DOS. Including vacancies reduces the density of states at the Fermi level and hence decreases the possibility of having a FM phase.

first-principles calculations of the CDW structure of monolayer VSe<sub>2</sub> also reported a distorted CDW structure more stable than the FM one, indicating a competition of magnetism and CDW.<sup>60</sup>

Following our XMCD data and DFT calculations, we have found a nonmagnetic ground state in monolayer VSe<sub>2</sub>, in agreement with recent ARPES data<sup>8,10</sup> that demonstrate the absence of spin-polarized bands in the monolayer limit.<sup>10</sup> More recent work<sup>58</sup> also reports a nonmagnetic but frustrated ground state in monolayer VSe<sub>2</sub> due to a competition between ferro- and antiferromagnetic orders. In addition, defects are shown to be detrimental to ferromagnetism, unlike the emergence of the vacancy-induced magnetism observed in graphite.<sup>22</sup> Although our magnetization data do not allow us to reveal a frustrated magnetic ground state, the absence of long-range magnetic order due to disorder and vacancies corroborates such magnetic frustration. Nevertheless, despite that our DFT calculations find a drop of DOS at the Fermi level discarding a possible FM state, the effect of intrinsic disorder in monolayer VSe<sub>2</sub> has to be carefully studied experimentally since high density of vacancies, antisites, substitutions, edges, and grain boundaries can dominate the material's properties.

In conclusion, we have studied experimentally and theoretically the ground state of bulk and monolayers of VSe<sub>2</sub>. Our DFT calculations predict that the ground state of bulk VSe<sub>2</sub> develops a commensurate lattice distortion with a  $4a \times 4a \times 3c$  supercell that reproduces the variation of the thermopower at high and low temperature, demonstrating the importance of considering the correct ground-state structure when performing *ab initio* studies in magnetic materials. This structure is shown to be related with the CDW phase that has been experimentally detected at low temperatures. Our DFT calculations for such a ground state show that FM is destroyed by such distortion, VSe<sub>2</sub> being a paramagnet in the bulk but on the verge to a magnetic state. This result confirms previous analysis that highlights the importance of phonon instabilities, besides electronic ones, in driving the formation of the CDW state.<sup>61</sup> It also reconciles theory and experiment. In the monolayer limit, we found that a periodic lattice distortion ( $2a \times 2a$ ) associated with the CDW

state is sufficient to open an energy gap through a Peierls-like distortion destroying the tendency toward a FM state, as we have reported experimentally by means of magnetization and XMCD. Our calculations suggest that the origin of the magnetic signal obtained for VSe<sub>2,0</sub> cannot be related to the band structure of the material, either in the bulk or in the single-layer limit, and any magnetic ground state in the monolayer limit might be associated with a high density of defects, edges, or grain boundaries, although control experiments in bulk VSe<sub>1.8</sub> and *ab initio* calculations in single-layer VSe<sub>2,0</sub> indicate that strain induced by vacancies works against ferromagnetism in clear contrast to the magnetic ground state recently reported in few-layer PtSe<sub>2</sub>,<sup>62</sup> presumably due to the strong competition between ferro- and antiferromagnetic states.<sup>58</sup>

## ■ AUTHOR INFORMATION

### Corresponding Authors

\*E-mail: adolfo.oterofumega@usc.es.

\*E-mail: victor.pardo@usc.es.

\*E-mail: sblanco@dipc.org.

### ORCID

C. Rogero: 0000-0002-2812-8853

P. Gargiani: 0000-0002-6649-0538

Victor Pardo: 0000-0002-4713-3519

### Notes

The authors declare no competing financial interest.

## ■ ACKNOWLEDGMENTS

This work is supported by the MINECO of Spain through the project MAT2016-80762-R, PGC2018-101334-A-C22, and PGC2018-101334-B-C21. A.O.F. thanks MECD for the financial support received through the FPU grant FPU16/02572. M.G. acknowledges funding from the European Commission through the Marie Skłodowska-Curie IEF project SUPER2D (GA-748971). M.M.U. acknowledges support by the Spanish MINECO under grant no. MAT2017-82074-ERC and by the ERC Starting grant LINKSPM (Grant 758558). A. Berger and L. H. Hueso are acknowledged for sharing CIC nanoGUNE facilities and the SQUID measurements. S.B.-C. thanks IKERBASQUE for financial support. We also thank J. Fernández-Rossier, I. Oleynik, Warren E. Pickett, and D. Soriano for fruitful discussions and ALBA Synchrotron Light Facility for the provision of synchrotron beamtime.

## ■ REFERENCES

- (1) Novoselov, K. S.; Geim, A. K.; Morozov, S. V.; Jiang, D.; Zhang, Y.; Dubonos, S. V.; Grigorieva, I. V.; Firsov, A. A. Electric Field Effect in Atomically Thin Carbon Films. *Science* **2004**, *306*, 666–669.
- (2) Manzeli, S.; Ovchinnikov, D.; Pasquier, D.; Yazev, O. V.; Kis, A. 2D transition metal dichalcogenides. *Nature Reviews Materials* **2017**, *2*, 17033.
- (3) Choi, W.; Choudhary, N.; Han, G. H.; Park, J.; Akinwande, D.; Lee, Y. H. Recent development of two-dimensional transition metal dichalcogenides and their applications. *Mater. Today* **2017**, *20*, 116–130.
- (4) Zhang, G.; Zhang, Y.-W. Thermoelectric properties of two-dimensional transition metal dichalcogenides. *J. Mater. Chem. C* **2017**, *5*, 7684–7698.
- (5) Xia, J.; Yan, J.; Shen, Z. X. Transition metal dichalcogenides: structural, optical and electronic property tuning via thickness and stacking. *FlatChem.* **2017**, *4*, 1–19.
- (6) Akinwande, D.; Petrone, N.; Hone, J. Two-dimensional flexible nanoelectronics. *Nat. Commun.* **2014**, *5*, 5678.

- (7) Xu, K.; Chen, P.; Li, X.; Wu, C.; Guo, Y.; Zhao, J.; Wu, X.; Xie, Y. Ultrathin Nanosheets of Vanadium Diselenide: A Metallic Two-Dimensional Material with Ferromagnetic Charge-Density-Wave Behavior. *Angew. Chem., Int. Ed.* **2013**, *52*, 10477–10481.
- (8) Feng, J.; et al. Electronic Structure and Enhanced Charge-Density Wave Order of Monolayer VSe<sub>2</sub>. *Nano Lett.* **2018**, *18*, 4493–4499.
- (9) Umemoto, Y.; Sugawara, K.; Nakata, Y.; Takahashi, T.; Sato, T. Pseudogap, Fermi arc, and Peierls-insulating phase induced by 3D–2D crossover in monolayer VSe<sub>2</sub>. *Nano Res.* **2019**, *12*, 165–169.
- (10) Chen, P.; Pai, W. W.; Chan, Y.-H.; Madhavan, V.; Chou, M. Y.; Mo, S.-K.; Fedorov, A.-V.; Chiang, T.-C. Unique Gap Structure and Symmetry of the Charge Density Wave in Single-Layer VSe<sub>2</sub>. *Phys. Rev. Lett.* **2018**, *121*, 196402.
- (11) Ugeda, M. M.; et al. Characterization of collective ground states in single-layer NbSe<sub>2</sub>. *Nat. Phys.* **2016**, *12*, 92.
- (12) Tran, K.; et al. Evidence for moiré excitons in van der Waals heterostructures. *Nature* **2019**, *567*, 71–75.
- (13) Seyler, K. L.; Rivera, P.; Yu, H.; Wilson, N. P.; Ray, E. L.; Mandrus, D. G.; Yan, J.; Yao, W.; Xu, X. Signatures of moiré-trapped valley excitons in MoSe<sub>2</sub>/WSe<sub>2</sub> heterobilayers. *Nature* **2019**, *567*, 66–70.
- (14) Jin, C.; Regan, E. C.; Yan, A.; Iqbal Bakti Utama, M.; Wang, D.; Zhao, S.; Qin, Y.; Yang, S.; Zheng, Z.; Shi, S.; Watanabe, K.; Taniguchi, T.; Tongay, S.; Zettl, A.; Wang, F. Observation of moiré excitons in WSe<sub>2</sub>/WS<sub>2</sub> heterostructure superlattices. *Nature* **2019**, *567*, 76–80.
- (15) Alexeev, E. M.; et al. Resonantly hybridized excitons in moiré superlattices in van der Waals heterostructures. *Nature* **2019**, *567*, 81–86.
- (16) Mermin, N. D.; Wagner, H. Absence of Ferromagnetism or Antiferromagnetism in One- or Two-Dimensional Isotropic Heisenberg Models. *Phys. Rev. Lett.* **1966**, *17*, 1133–1136.
- (17) Huang, B.; Clark, G.; Navarro-Moratalla, E.; Klein, D. R.; Cheng, R.; Seyler, K. L.; Zhong, D.; Schmidgall, E.; McGuire, M. A.; Cobden, D. H.; Yao, W.; Xiao, D.; Jarillo-Herrero, P.; Xu, X. Layer-dependent ferromagnetism in a van der Waals crystal down to the monolayer limit. *Nature* **2017**, *546*, 270–273.
- (18) Burch, K. S.; Mandrus, D.; Park, J.-G. Magnetism in two-dimensional van der Waals materials. *Nature* **2018**, *563*, 47–52.
- (19) Gibertini, M.; Koperski, M.; Morpurgo, A. F.; Novoselov, K. S. Magnetic 2D materials and heterostructures. *Nat. Nanotechnol.* **2019**, *14*, 408–419.
- (20) Alloul, H.; Bobroff, J.; Gabay, M.; Hirschfeld, P. J. Defects in correlated metals and superconductors. *Rev. Mod. Phys.* **2009**, *81*, 45–108.
- (21) Praetorius, C.; Fauth, K. Kondo screening and beyond: An x-ray absorption and dichroism study of CePt<sub>5</sub>/Pt(111). *Phys. Rev. B: Condens. Matter Mater. Phys.* **2017**, *95*, 115113.
- (22) Červenka, J.; Katsnelson, M.; Flipse, C. Room-temperature ferromagnetism in graphite driven by two-dimensional networks of point defects. *Nat. Phys.* **2009**, *5*, 840.
- (23) Yazyev, O. V.; Helm, L. Defect-induced magnetism in graphene. *Phys. Rev. B: Condens. Matter Mater. Phys.* **2007**, *75*, 125408.
- (24) Bonilla, M.; Kolekar, S.; Ma, Y.; Diaz, H. C.; Kalappattil, V.; Das, R.; Eggers, T.; Gutierrez, H. R.; Phan, M.-H.; Batzill, M. Strong room-temperature ferromagnetism in VSe<sub>2</sub> monolayers on van der Waals substrates. *Nat. Nanotechnol.* **2018**, *13*, 289.
- (25) Gong, C.; Li, L.; Li, Z.; Ji, H.; Stern, A.; Xia, Y.; Cao, T.; Bao, W.; Wang, C.; Wang, Y.; Qiu, Z.; Cava, R.; Louie, S. G.; Xia, J.; Zhang, X. Discovery of Intrinsic Ferromagnetism in Two-Dimensional van der Waals Crystals. *Nature* **2017**, *546*, 265.
- (26) Guo, Y.; Deng, H.; Sun, X.; Li, X.; Zhao, J.; Wu, J.; Chu, W.; Zhang, S.; Pan, H.; Zheng, X.; Wu, X.; Jin, C.; Wu, C.; Xie, Y. Modulation of Metal and Insulator States in 2D Ferromagnetic VS<sub>2</sub> by van der Waals Interaction Engineering. *Adv. Mater.* **2017**, *29*, 1700715.
- (27) Bussmann-Holder, A.; Bttner, H. Charge-density-wave formation in TiSe<sub>2</sub> driven by an incipient antiferroelectric instability. *J. Phys.: Condens. Matter* **2002**, *14*, 7973.
- (28) Wilson, J. A.; Di Salvo, F. J.; Mahajan, S. Charge-density waves and superlattices in the metallic layered transition metal dichalcogenides. *Adv. Phys.* **1975**, *24*, 117–201.
- (29) Van Bruggen, C. F.; Haas, C. Magnetic susceptibility and electrical properties of VSe<sub>2</sub> single crystals. *Solid State Commun.* **1976**, *20*, 251–254.
- (30) Yadav, C.; Rastogi, A. Electronic transport and specific heat of. *Solid State Commun.* **2010**, *150*, 648–651.
- (31) Williams, P. M.; Scruby, C. B.; Clark, W. B.; Parry, G. S. Charge density waves in the layered transition metal dichalcogenides. *Le Journal de Physique Colloques* **1976**, *37*, C4-139.
- (32) Eaglesham, D. J.; Withers, R. L.; Bird, D. M. Charge-density-wave transitions in 1T-VSe<sub>2</sub>. *J. Phys. C: Solid State Phys.* **1986**, *19*, 359.
- (33) Woolley, A. M.; Wexler, G. Band structures and Fermi surfaces for 1T-TaS<sub>2</sub>, 1T-TaSe<sub>2</sub> and 1T-VSe<sub>2</sub>. *J. Phys. C: Solid State Phys.* **1977**, *10*, 2601.
- (34) Strocov, V. N.; Shi, M.; Kobayashi, M.; Monney, C.; Wang, X.; Krempasky, J.; Schmitt, T.; Patthey, L.; Berger, H.; Blaha, P. Three-Dimensional Electron Realm in VSe<sub>2</sub> by Soft-X-Ray Photoelectron Spectroscopy: Origin of Charge-Density Waves. *Phys. Rev. Lett.* **2012**, *109*, 086401.
- (35) Bayard, M.; Sienko, M. Anomalous electrical and magnetic properties of vanadium diselenide. *J. Solid State Chem.* **1976**, *19*, 325–329.
- (36) Barua, S.; Hatnean, M. C.; Lees, M. R.; Balakrishnan, G. Signatures of the Kondo effect in VSe<sub>2</sub>. *Sci. Rep.* **2017**, DOI: 10.1038/s41598-017-11247-4.
- (37) Cao, Q.; Yun, F. F.; Sang, L.; Xiang, F.; Liu, G.; Wang, X. Defect introduced paramagnetism and weak localization in two-dimensional metal VSe<sub>2</sub>. *Nanotechnology* **2017**, *28*, 475703.
- (38) Li, F.; Tu, K.; Chen, Z. Versatile Electronic Properties of VSe<sub>2</sub> Bulk, Few-Layers, Monolayer, Nanoribbons, and Nanotubes: A Computational Exploration. *J. Phys. Chem. C* **2014**, *118*, 21264–21274.
- (39) Ma, Y.; Dai, Y.; Guo, M.; Niu, C.; Zhu, Y.; Huang, B. Evidence of the Existence of Magnetism in Pristine VX<sub>2</sub> Monolayers (X = S, Se) and Their Strain-Induced Tunable Magnetic Properties. *ACS Nano* **2012**, *6*, 1695–1701.
- (40) Esters, M.; Hennig, R. G.; Johnson, D. C. Dynamic instabilities in strongly correlated VSe<sub>2</sub> monolayers and bilayers. *Phys. Rev. B: Condens. Matter Mater. Phys.* **2017**, *96*, 235147.
- (41) Fuh, H.-R.; Yan, B.; Wu, S.-C.; Felser, C.; Chang, C.-R. Metal-insulator transition and the anomalous Hall effect in the layered magnetic materials VS<sub>2</sub> and VSe<sub>2</sub>. *New J. Phys.* **2016**, *18*, 113038.
- (42) Barla, A.; Nicolás, J.; Cocco, D.; Valvidares, S. M.; Herrero-Martín, J.; Gargiani, P.; Moldes, J.; Ruget, C.; Pellegrin, E.; Ferrer, S. Design and performance of BOREAS, the beamline for resonant X-ray absorption and scattering experiments at the ALBA synchrotron light source. *J. Synchrotron Radiat.* **2016**, *23*, 1507–1517.
- (43) Haverkort, M. W.; Zwierzycki, M.; Andersen, O. K. Multiplet ligand-field theory using Wannier orbitals. *Phys. Rev. B: Condens. Matter Mater. Phys.* **2012**, *85*, 165113.
- (44) Lu, Y.; Höppner, M.; Gunnarsson, O.; Haverkort, M. W. Efficient real-frequency solver for dynamical mean-field theory. *Phys. Rev. B: Condens. Matter Mater. Phys.* **2014**, *90*, 085102.
- (45) Hohenberg, P.; Kohn, W. Inhomogeneous Electron Gas. *Phys. Rev.* **1964**, *136*, B864–B871.
- (46) Kohn, W.; Sham, L. J. Self-Consistent Equations Including Exchange and Correlation Effects. *Phys. Rev.* **1965**, *140*, A1133–A1138.
- (47) Schwarz, K.; Blaha, P. Solid state calculations using WIEN2k. *Comput. Mater. Sci.* **2003**, *28*, 259–273.
- (48) Perdew, J. P.; Burke, K.; Ernzerhof, M. Generalized Gradient Approximation Made Simple. *Phys. Rev. Lett.* **1996**, *77*, 3865–3868.
- (49) Anisimov, V. I.; Aryasetiawan, F.; Lichtenstein, A. I. First-principles calculations of the electronic structure and spectra of strongly correlated systems: the LDA+U method. *J. Phys.: Condens. Matter* **1997**, *9*, 767.
- (50) Madsen, G. K.; Carrete, J.; Verstraete, M. J. BoltzTraP2, a program for interpolating band structures and calculating semi-classical transport coefficients. *Comput. Phys. Commun.* **2018**, *231*, 140–145.

- (51) Barua, S.; Hatnean, M. C.; Lees, M. R.; Balakrishnan, G. Signatures of the Kondo effect in VSe<sub>2</sub>. *Sci. Rep.* **2017**, *7*, 10964.
- (52) Grüner, G. *Charge Density Waves in Solids*; Addison-Wesley, 1994.
- (53) Terashima, K.; Sato, T.; Komatsu, H.; Takahashi, T.; Maeda, N.; Hayashi, K. Charge-density wave transition of 1 T  $\hat{\wedge}$  VSe<sub>2</sub> studied by angle-resolved photoemission spectroscopy. *Phys. Rev. B: Condens. Matter Mater. Phys.* **2003**, DOI: 10.1103/PhysRevB.68.155108.
- (54) Stoner, E. C. Collective electron ferronmagnetism. *Proceedings of the Royal Society of London A: Mathematical, Physical and Engineering Sciences* **1938**, *165*, 372–414.
- (55) Moriya, T. *Spin fluctuations in itinerant electron magnetism*; Springer Series in Solid-State Sciences; Springer-Verlag, 1985.
- (56) Fritzsche, L.; Weimert, B. First-Principles Theory of Ferromagnetic and Antiferromagnetic Order. *Phys. Status Solidi B* **1998**, *208*, 287–337.
- (57) Zhang, W.; Zhang, L.; Wong, P. K. J.; Yuan, J.; Vinai, G.; Torelli, P.; van der Laan, G.; Feng, Y. P.; Wee, A. T. S. Magnetic Transition in Monolayer VSe<sub>2</sub> via Interface Hybridization. *ACS Nano* **2019**, *13*, 8997.
- (58) Wong, P. K. J.; et al. Evidence of Spin Frustration in a Vanadium Diselenide Monolayer Magnet. *Adv. Mater.* **2019**, *31*, 1901185.
- (59) Haverkort, M. Spin and orbital degrees of freedom in transition metal oxides and oxide thin films studied by soft x-ray absorption spectroscopy. *Ph.D. thesis*; Universität zu Köln, 2005.
- (60) Coelho, P. M.; Nguyen Cong, K.; Bonilla, M.; Kolekar, S.; Phan, M.-H.; Avila, J.; Asensio, M. C.; Oleynik, I. I.; Batzill, M. Charge Density Wave State Suppresses Ferromagnetic Ordering in VSe<sub>2</sub>Monolayers. *J. Phys. Chem. C* **2019**, *123*, 14089–14096.
- (61) Johannes, M. D.; Mazin, I. I. Fermi surface nesting and the origin of charge density waves in metals. *Phys. Rev. B: Condens. Matter Mater. Phys.* **2008**, *77*, 165135.
- (62) Avsar, A.; Ciarrocchi, A.; Pizzochero, M.; Unuchek, D.; Yazhev, O. V.; Kis, A. Defect induced, layer-modulated magnetism in ultrathin metallic PtSe<sub>2</sub>. *Nat. Nanotechnol.* **2019**, *14*, 674–678.